Indian Journal of Chemical Technology
Vol. 30, March 2023, pp. 198-204
DOI: 10.56042/ijct.v30i2.68707

Synthesis of high temperature resistant ZrO_2-SiO_2 composite aerogels via supercritical fluid deposition

Xiaoqing Wang*,[1] & Chengyuan Li [2]

[1]College of Materials and Chemical Engineering, Chuzhou University, Huifeng West Road 1, Chuzhou 239 000, China,
[2]Intel Semiconductor Storage Technology (Dalian) Co., Ltd, Huaihe East Road 109, Dalian 116 000, China.

E-mail: xiaoqingwang2013@chzu.edu.cn.

Received 15 November 2022; accepted 25 January 2023

A series of ZrO_2-SiO_2 composite aerogels have been synthesized by adjusting the volume of tetraethoxysilane (TEOS) during supercritical fluid drying process. ZrO_2 aerogels have been prepared via the sol-gel reaction using $ZrOCl_2 \cdot 8H_2O$ and the gel initiator malic acid as raw materials. Then the ZrO_2-SiO_2 composite aerogels have been obtained by supercritical fluid deposition (SCFD). The samples have been characterized applying XRD, FTIR, SEM, TEM, TGA and Nitrogen adsorption-desorption. The introduction of SiO_2 can effectively restrain the growth of the nanoparticles and the transformation of crystalline phase, and reduce the linear shrinkage of the aerogels. It indicates the improvement of the thermostability of the ZrO_2-SiO_2 composite aerogels.

Keywords: Aerogel, Sol-gel, Supercritical fluid deposition, ZrO_2-SiO_2

ZrO_2 aerogel with low density and high porosity have enormous application prospects as the next generation of high temperature resistant material [1]. And the high melting point of zirconia materials is ~2700°C. ZrO_2 aerogels became irreplaceable materials in space exploration[2]. Therefore, more and more attention has been paid to zirconia aerogel. But the resistance to high temperature of ZrO_2 in practical application is still insufficient, such as the tolerance of thermal stability under 1200 °C[2, 3].

Seeking for better performance of ZrO_2 in the practical engineering application, researchers have done lots of modified work with respect to this problem. Composite aerogels were prepared, including ZrO_2-Al_2O_3, ZrO_2-SiO_2, ZrO_2-TiO_2, and so on[4-7]. ZrO_2-SiO_2 aerogels were mainly synthesized by three methods. One was ZrO_2 modified with TEOS [8, 9]. One was using sodium silicate (Na_2SiO_3) as a gelation agent in zirconia sol-gel reactions[10]. Another was by "click" reaction to form new organic acid to in-situ hydrolysis of silicon source[11]. After modified, the grain growth and linear shrinkage problem of ZrO_2 aerogel have been restricted. For example, Shen's group developed the sol-gel method to effectively control the hydrolysis rate of zirconium butoxide by acetone-aniline in situ water formation. Then the liquid phase deposition technology was applied in the process of aging. The obtained composite aerogel ZrO_2-SiO_2 had good heat resistance and mechanical strength. The specific surface area of the composite aerogel was 186 m^2/g and line shrinkage rate of 10%[12]. Furthermore, the ZrO_2 nanoparticles were also modified by coating with silica during the aging process. The wet gel was aged in TEOS and Fe (III) solution by repetition to obtain the Fe (III) modified ZrO_2/SiO_2 composite aerogel. Further research was developed to modify ZrO_2 with SiO_2 during supercritical drying process[13]. The particle size and specific surface area of organic-inorganic modified ZrO_2/SiO_2 composite aerogel after 1000°C heat treatment were 3~4 nm and 203.5 m^2/g, respectively. This method needed to replace aging solution by repetition, and needed the toxic hexamethyldisiloxane as silicon source.

It was reported that the side group and -COOH in organic acids can bind Zr^{4+} to form wet gels[14-17]. Based on these results, the green organic acid---L-malic acid (LMA) was chosen as a gelator to facilitate $ZrOCl_2$ to form gel. Then different amounts of TEOS were adopted in the process of supercritical drying to obtain ZrO_2-SiO_2 composite aerogel. When the composite aerogels were treated at 1000°C, the linear shrinkage decreased significantly from 52% to 20%. It should be attributed to the introduction of SiO_2, inhibited the grain growth and transformation of the aerogel after heat treatment.

Experimental Section

Materials and Reagents

All chemical reagents were analytically pure and were used as received without further purification, including zirconium oxychloride ($ZrOCl_2 \cdot 8H_2O$, 99.9%, Aladdin, China), L-malic acid (LMA, $C_4H_6O_5$, 98%, Aladdin, China), tetraethoxysilane (TEOS, Sinopharm Chemical Reagent Co, Ltd (SCRC)) and absolute ethanol (EtOH, Sinopharm Chemical Reagent Co, Ltd (SCRC)).

Preparation of zirconia wet gel

In a typical preparation procedure, 0.46 mol/L of $ZrOCl_2 \cdot 8H_2O$ (A solution) and 1.0 mol/L of LMA (B solution) ethanol colourless and transparent solution were prepared. A given volume (2-6 mL) of B solution was then quickly added into A solution under continuous stirring. The solution was then transferred to sealed glass culture dishes at 60°C to form the wet gels. The detailed experimental data were listed in Table 1.

[a] LMA-2-aerogel means the volume of the LMA was 2 mL.

[b]LMA-2-V5-aerogel means the volume of the LMA was 2 mL, the volume of TEOS was 5 mL.

Preparation of ZrO_2 and ZrO_2-SiO_2 composite aerogel

The wet gels were aged in EtOH for 3 days, then transferred into an autoclave. The supercritical fluid was EtOH or a mixture of EtOH and TEOS (V/V =300 mL: 5/10/30 mL). The final temperature and pressure of the system were 260°C and 7 MPa. The supercritical state was maintained for 65 min, and the autoclave was decompressed to atmospheric pressure and cooled to room temperature, then the composite aerogels were obtained, which were named LMA-X-VY-aerogel (X: the volume of LMA, Y: the volume of TEOS).

Table 1— The preparation parameters of the modified ZrO_2 aerogels

Samples	LMA (mL)	TEOS (mL)
LMA-2-aerogel[a]	2	0
LMA-3-aerogel	3	0
LMA-4-aerogel	4	0
LMA-5-aerogel	5	0
LMA-6-aerogel	6	0
LMA-2-V5-aerogel [b]	2	5
LMA-3-V5-aerogel	3	5
LMA-4-V5-aerogel	4	5
LMA-5-V5-aerogel	5	5
LMA-6-V5-aerogel	6	5
LMA-2-V10-aerogel	2	10
LMA-3-V10-aerogel	3	10
LMA-4-V10-aerogel	4	10
LMA-5-V10-aerogel	5	10
LMA-6-V10-aerogel	6	10
LMA-2-V30-aerogel	2	30
LMA-3-V30-aerogel	3	30
LMA-4-V30-aerogel	4	30
LMA-5-V30-aerogel	5	30
LMA-6-V30-aerogel	6	30

Characterization

The morphology of the aerogels was observed by HITACHIS-4800 scanning electron microscope (SEM) and transmission electron microscopy (TEM, Tecnai G^2F20 S-TWINFEI) equipped with Energy-dispersive X-ray spectroscopy (EDX). X-ray diffraction (XRD) measurement was performed in an X-ray diffractometer (X'Pert PRO, PANalytical B.V.) with Cu K_α radiation (λ = 1.5418 Å) at 4°/min scanning speed in the 2θ range from 10° to 90°. Thermogravimetric analysis (TGA) and differential thermal analysis (DTA) are performed on a TA-Q 500 TGA instrument. Samples are pre-treated at 100 °C for 30 minutes before being heated to 1000 °C (10 °C /min). Fourier Transform Infrared Spectroscopy (FT-IR) was recorded on Nicolet 5700 spectrophotometer using KBr pellets containing 1 wt% of samples. Nitrogen adsorption-desorption measurements (Quantachrome Instrument Corp) were performed at 77 K. Surface area is evaluated using the Brunauer-Emmett-Teller (BET) method from the adsorption branch of the isotherm curve. The pore-size distributions were calculated according to the Barrett-Joyner-Halenda (BJH) model. The average pore diameters and cumulative pore volumes were calculated using the desorption branch of the isotherm.

Results and Discussion

FT-IR analysis

The FT-IR spectra of LMA-6-aerogel, LMA-6-V10-aerogelandLMA-6-V30-aerogel were shown in Fig. 1. The band located at 3434 cm^{-1} in both spectra was attributed to the -OH vibration of the samples and the adsorbed water on their surfaces[18,19]. The absorbance of ν_{as} (C=O) vibration was located at 1632 and 1634 cm^{-1} [20-22]. It is known that SiO_2 should exist in LMA-6-V10-aerogel and LMA-6-V30-aerogel. Specifically, the characteristic band at 1067 cm^{-1} was assigned to Si-O in LMA-6-V10-aerogel and LMA-6-V30-aerogel[18,23], indicating that SiO_2 has successfully incorporated into ZrO_2 during SCFD process.

SEM analysis

The SEM images of LMA-6-aerogel and LMA-6-V30-aerogel were showed in Fig. 2 (a and b). After the heat treatment at 1000°C, the particle size of LMA-6-aerogel-1000 was about 40-65 nm, which was increased obviously. While there was no obvious change in LMA-6-V30-aerogel-1000, the particle size was about 10-15 nm, which was seen in Fig. 2 (c and d). This should be attributed to the SiO_2 phase introduced in SCFD process. The introduced SiO_2 was an effective inhibitor to restrain the growth of nanoparticles of the aerogel[19, 22, 24, 25]. The particle size measured by SEM characterization differed from the numerical values calculated by XRD data using Scherer equation and the TEM results. The SEM results were too large. It can be attributed to the agglomerative tendency of the prepared aerogels, and its poor electrical conductivity, led to the SEM graphs not very clear to distinguish each nanoparticle. The photographs of LMA-6-aerogel and LMA-6-V30-aerogel show that the diameter of LMA-6-aerogel and LMA-6-V30-aerogel were about 4 cm and 5 cm, respectively. When they were treated at 1000°C for 1 hour, the diameter of LMA-6-aerogel shrank to 2 cm, while LMA-6-V30-aerogel 4 cm. The linear shrinkage of the two aerogels was about 50 and 20% by calculation.

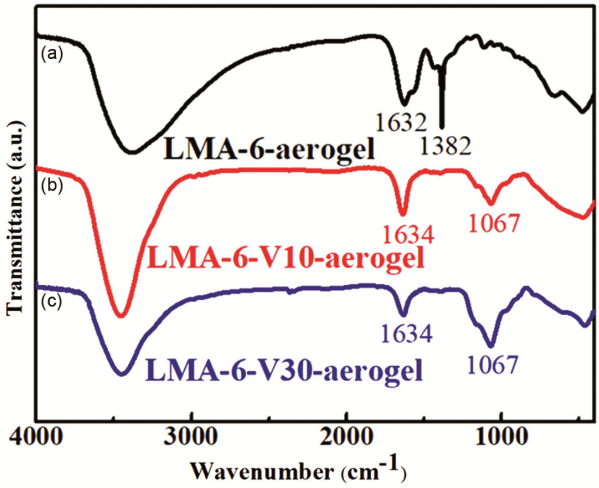

Fig. 1 — FT-IR spectra of (a) LMA-6-aerogel; (b) LMA-6-V10-aerogel and (c) LMA-6-V30-aerogel

TEM analysis

TEM characterization was applied to further investigate the morphology and the thermal stability of the prepared aerogels. The microstructure of the LMA-6-aerogel and LMA-6-VX-aerogel (X = 5, 10, 30) samples before and after heat-treatment at 1000 °C were showed in Fig. 3. The morphology of the as-prepared aerogels before heat-treatment was similar with each other. From the images in Fig. 3 (a, c, e, g), it can be seen that all of them showed randomly interconnected networks with irregular sphere nanoparticles. However, when the four samples were

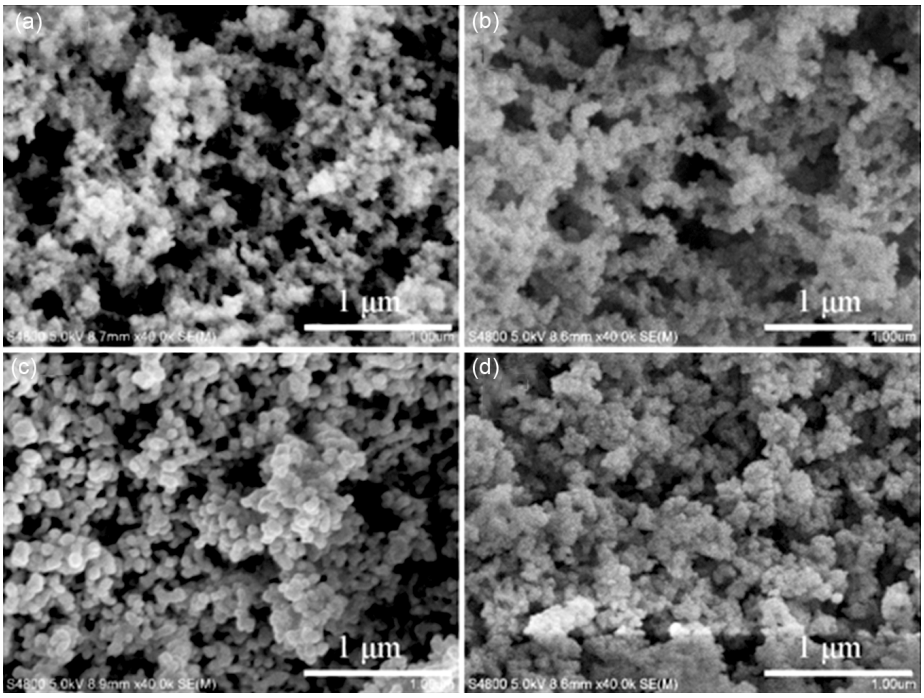

Fig. 2 — SEM images of aerogel (a)LMA-6-aerogel; (b) LMA-6-V30-aerogel; (c) LMA-6-aerogel-1000 and (d) LMA-6-V30-aerogel-1000

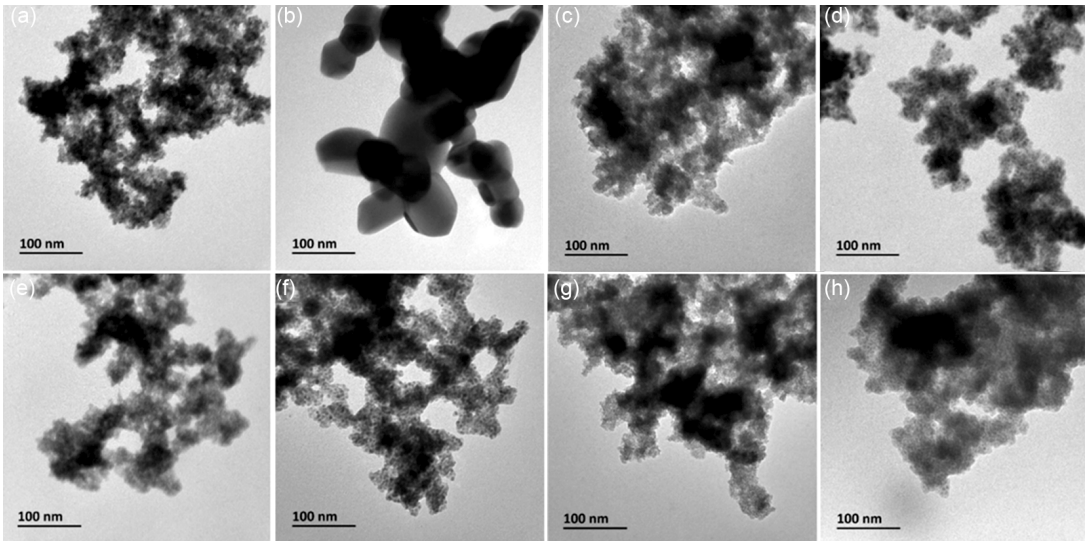

Fig. 3 — TEM images of aerogel (a) LMA-6-aerogel; (b) LMA-6-aerogel-1000; (c) LMA-6-V5-aerogel; (d) LMA-6-V5-aerogel-1000; (e) LMA-6-V10-aerogel; (f) LMA-6-V10-aerogel-1000; (g) LMA-6-V30-aerogel and (h) LMA-6-V30-aerogel-1000

treated at 1000°C for 1 h, there was dramatic difference to LMA-6-aerogel-1000 and LMA-6-VX-aerogel-1000 (X = 5, 10, 30) samples.

From the images in Fig. 3 (b, d, f, h), it can be seen that the particle size in LMA-6-aerogel-1000 was obvious larger than that in LMA-6-VX-aerogel-1000 (X = 5, 10, 30). The particle growth in LMA-6 after heating treatment was evident, which was attributed to the nanoparticles sintering during the heat-treatment process. And the particle size was estimated to be ~60 nm. While the particle size in LMA-6-VX-aerogel-1000 (X = 5, 10, 30) was about 5-8 nm, much smaller, which was almost no obvious variation in comparison with LMA-6-VX-aerogel (X = 5, 10, 30). Obviously, it was accounted to the SiO_2 phase introduced the aerogels in the SCFD process. The composite aerogels formed core-shell structure. The successful introduction of SiO_2 as shell inhibited the growth of micro crystals under thermal treatment. There are some literatures reported SiO_2 improved the thermal stability of ZrO_2. SiO_2 was introduced in aging process to improve the compressive strength of ZrO_2-SiO_2 aerogel[19]. ZrO_2-SiO_2 aerogel was obtained via SCFD process, and the particle size of the ZrO_2-SiO_2-1000 aerogel was restricted to 10-30 nm [22]. Therefore, the introduction of SiO_2 can improve the thermal stability of ZrO_2 aerogel.

XRD analysis

The thermal stability of LMA-6-V30-aerogel was much higher than the sample LMA-6-aerogel (X = 2, 3, 4, 5) via the above analysis. The XRD characterization was further applied to evaluate the thermal stability of the samples, which was shown in Fig. 4 and Fig. S2. From the images in Fig. 4a, it can

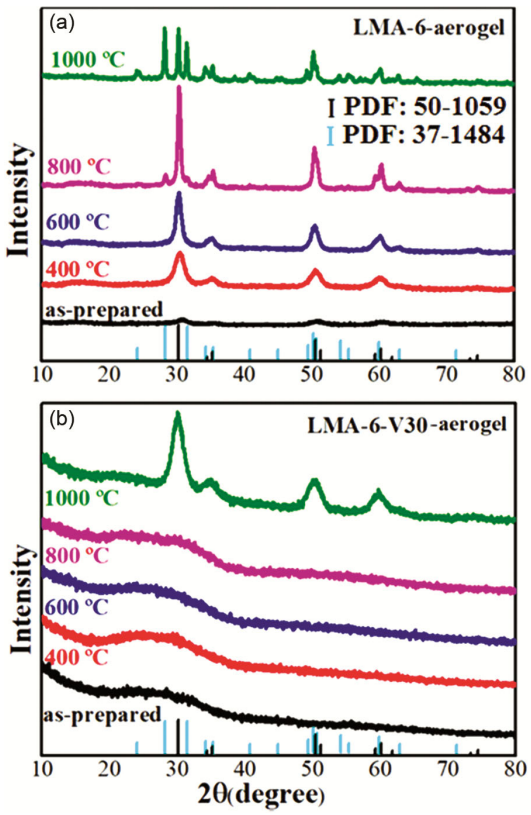

Fig. 4 — XRD patterns of (a) LMA-6-aerogel; (b) LMA-6-V30-aerogel (for the as prepared sample and samples after calcination at different temperature for 1 hour)

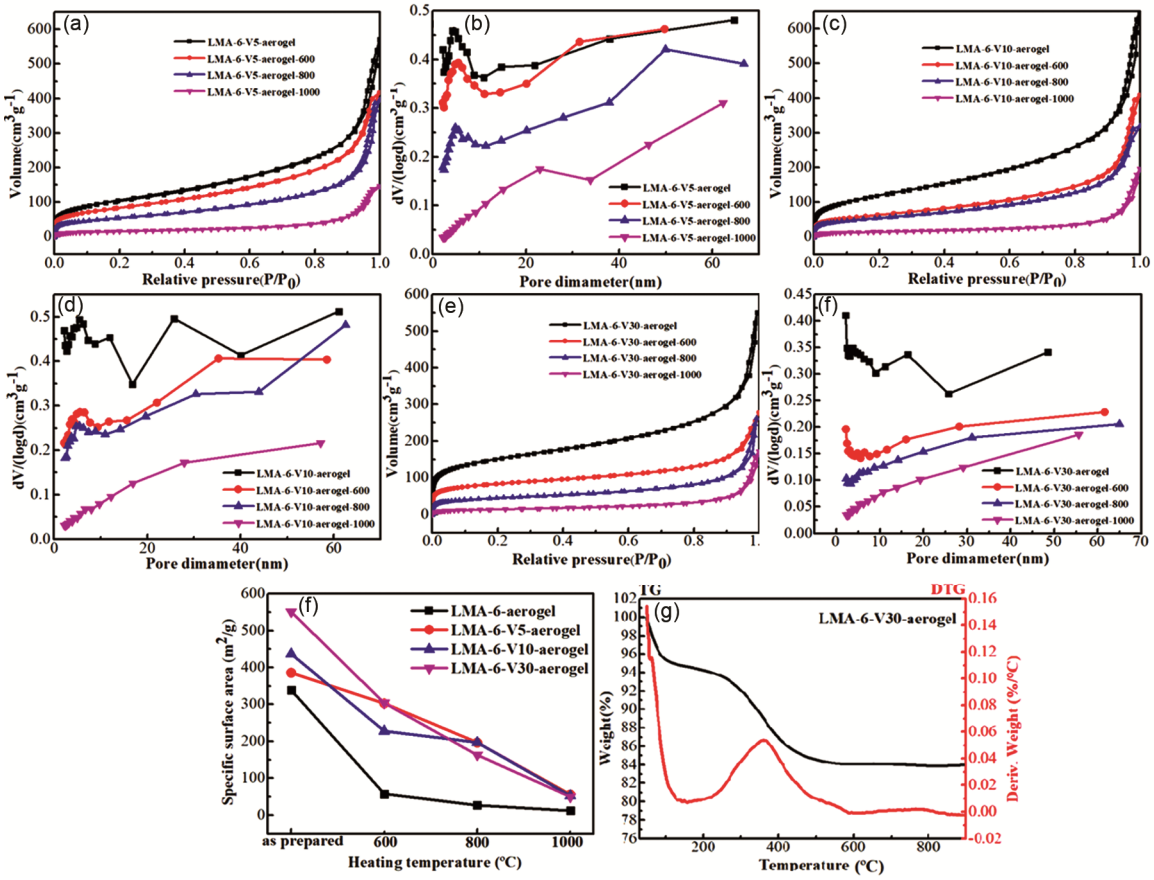

Fig. 5 — (a, c, e) Nitrogen adsorption-desorption isotherms of LMA-6-VX-aerogel (X = 5, 10, 30) as-prepared and that were heated at 600, 800 and 1000 °C; (b, d, f) Pore size distributions isotherms of LMA-6-VX-aerogel (X = 5, 10, 30) as-prepared and that were heated at 600, 800 and 1000 °C; (g) Specific surface area of LMA-6-VX-aerogel (X = 5, 10, 30) calcined at different temperature and (h) TG-DTG curve of aerogel of LMA-6-V30-aerogel

be seen that the as-prepared LMA-6-aerogel was amorphous. It was tetragonal phase under 600 °C, and the diffraction peaks were at around 30.27°, 34.81°, 50.38° and 59.61°(JCPDS card no. 50-1089). Monoclinic phase was detected at 800 and 1000 °C, and its main peaks were at about 24°, 28.2°, 31.5° and 54° (JCPDS card no. 37-1484)[26, 27]. In stark contrast to LMA-6-aerogel, the XRD patterns of LMA-6-VX-aerogel (X = 5, 10, 30) were amorphous phase below 800 °C, which showed broad diffraction peaks (Fig. 4b). From the images, it can be seen that phase transformation of LMA-6-VX-aerogel (X = 5, 10, 30) took place only at 1000 °C. The X-ray crystallinity and crystallite size were calculated by Scherer equation. All the samples were calculated by tetragonal phase. The detailed results were listed in Table 2. From Table 2, it can be seen that the X-ray crystallinity and crystallite size gradually decreased, demonstrating the introduction of SiO_2 can inhibit the growth of the particles. Meanwhile, the X-ray crystallinity of sample LMA-6-V30-aerogel-1000 was 24.9%, and it was smallest. It illustrated the better retention of amorphous state with the increase of SiO_2. By comparison with the XRD results, it was discovered that the thermal stability of the aerogel improved tremendously when SiO_2 was introduced into ZrO_2, which was closed to the TEM results.

N_2 adsorption-desorption analysis

N_2 adsorption-desorption characterizations were applied to detect the surface area and pore volume of LMA-6-aerogel and LMA-6-VX-aerogel (X = 5, 10, 30) as-prepared and that were treated at 1000 °C, and the results were listed in Fig. 5 (a-f) and Table 2. All the as-prepared four samples showed similar Type II isothermal curves, shown in Fig. 5 (a, c and e). The specific surface areas of LMA-6-aerogel and LMA-6-VX-aerogel (X = 5, 10, 30) as-prepared were 339, 386, 437 and 551 m^2/g, respectively. The specific

Table 2 — Surface area, pore volume and linear shrinkage of LMA-6 and LMA-6-VX-aerogel (X = 5, 10, 30) as-prepared and that treated at 1000 °C

samples	Surface area (m^2/g)	Pore volume (cm^3/g)	linear shrinkage (ΔL/L)	X-ray crystallinity	crystallite size calculated by Scherer equation（nm）
LMA-6-aerogel	339	0.92	/	/	/
LMA-6-aerogel-1000	12	0.06	52%	78.6%	30.8
LMA-6-V5-aerogel	386	0.88	/	/	/
LMA-6-V5-aerogel-1000	56	0.23	41%	43.0%	5.6
LMA-6-V10-aerogel	437	1.00	/	/	/
LMA-6-V10-aerogel-1000	53	0.30	37%	39.9%	5.2
LMA-6-V30-aerogel	551	0.85	/	/	/
LMA-6-V30-aerogel-1000	50	0.27	20%	24.9%	4.2

surface areas of LMA-6-VX-aerogel series were larger than that of LMA-6-aerogel, which were assigned to the introduction of SiO_2. Fig. 5 (b, d and f) gave the analysis of the mesopore size distribution accomplished by BJH method. The pore volumes of the as-prepared four samples had little difference, from 0.85 to 1.00 cm^3/g. According to the pore distribution cures, most of the pores were in the range of 2-40 nm. However, the surface area of the aerogels dropped significantly when treated at 1000°C, which was shown in Fig. 5g.

Comparing LMA-6-aerogel-1000 and LMA-6-VX-aerogel-1000 (X = 5, 10, 30), the surface area of the former was only 12 m^2/g, while the series of the latter were about 50-56 m^2/g. And for LMA-6-aerogel-1000, the pore volume reduced to 0.06 cm^3/g, while for LMA-6-VX-aerogel-1000, the pore volume reduced to 0.23-0.30 cm^3/g as shown in Fig. 5 (b, d and f). The results demonstrated the thermal stability of the series of LMA-6-VX-aerogel much improved. This result and the reported data in literatures were comparable. The surface area of the sulfated ZrO_2 aerogel was approximately 74 m^2/g after heat treatment at 700 °C [28]. The surface area of the ZrO_2/Y_2O_3 aerogel were 159 m^2/g and 26 m^2/g afterheat treatment at 550 and 1000 °C, respectively[29]. Comparing the data in Table 2, it can be discovered that LMA-6-V30-aerogel had the largest specific surface area of 551 m^2/g and the smallest linear shrinkage of 30%, indicating the good thermal stability of this sample. Therefore, LMA-6-V30-aerogel was chosen as the main research object. Such data evidenced the thermal stability was improved via the role of SiO_2.

TGA/DTA analysis

Figure 5h showed the TGA/DTA result of LMA-6-V30-aerogel. The sample was lost about 7 wt% weight loss at 50-250°C, corresponding to the surface adsorbed water and part of organics on the particle surface. There was about 10 wt% weight loss from 250 to 600 °C, which was mainly attributed to the decomposition of residual organics. And there was almost no weight loss from 600 to 900 °C, which was match with the FT-IR results.

Conclusion

ZrO_2-SiO_2 composite aerogels were successfully prepared by sol-gel method applying $ZrOCl_2 \cdot 8H_2O$, LMA and TEOS as raw materials followed by supercritical fluid deposition. The structural, morphological and specific surface area were investigated. The investigations made on the present study were:

IR spectra of LMA-6-VX-aerogel (X = 10, 30) showed absorption peak at 1067 cm^{-1} belonging to SiO_2, while LMA-6-aerogel did not present absorption peak at 1067 cm^{-1}, indicating the successful incorporation of SiO_2 into ZrO_2.

SEM analysis showed aerogels were made up of agglomerated nanoparticles. Compared with LMA-6-aerogel-1000,t e particle size of LMA-6-VX-aerogel-1000 were about 10-15 nm, having a little change before and after heating, which indicated the incorporation of SiO_2 can inhibit the nanoparticles' growth.

TEM analysis showed the core-shell structure in LMA-6-VX-aerogel. The shell SiO_2 can prevent the growth of the nanoparticles.

In XRD analysis, LMA-6-aerogel sample showed tetragonal phase at 400 °C. While the LMA-6-VX-aerogel samples(X = 5, 10, 30) kept amorphous phase under 800 °C, and it showed tetragonal phase until 1000 °C, demonstrating the latter had better heat stability.

N_2 adsorption-desorption characterizations showed the specific surface area of LMA-6-VX-aerogel-1000 samples were about 50 m^2/g, while LMA-6-aerogel-

1000 was 12 m^2/g, which was also responsible for the incorporation of SiO_2.

TGA/DTA results showed there was 20% other components including absorption water and the remaining organic acids above 600 °C in accordance with the FT-IR results.

In summary, comparing to LMA-6-aerogel, the heat stability of LMA-6-VX-aerogel has improved greatly. The size growth, linear shrinkage and the phase transformation of the aerogels were effectively restricted by incorporation of SiO_2 into ZrO_2. This preparation method was simple, and it supplied a way to improve the thermal stability of ZrO_2 aerogel.

Acknowledgements

This work is supported by the school fund (Grant No. 2020qd10), and General Natural Science Research Projects of Colleges and Universities in Anhui Province (Grant No. KJ2021B14).

Conflicts of author

The authors declare that they have no conflict of interest.

References

1 Walker R C, Potochniak A E, Hyer A P & Ferri J K, *Adv Colloid Interface Sci*, 295 (2021) 102464.
2 Shalygin A S, Katcin A A, Barnyakov A Y, Danilyuk A F & Martyanov O N, *Ceram Int*, 47 (2021) 9585.
3 Berardi U, Nanotech *Eco-Efficient Construct*, (2019) 395.
4 Gao B, Sun X, Yao C & Mao L, *J Solid State Chem*, 314 (2022) 123384.
5 Zhang X, Cheng X, Si Y, Yu J & Ding B, *Chem Eng J*, 433 (2022) 133268.
6 Dong J, Xie Y, Liu L, Deng Z, Liu W, Zhu L, Wang X, Xu D & Zhang G, *Adv Eng Mat*, 24 (2022) 2101603.
7 Yu H, Jiang Y, Lu Y, Li X, Zhao H, Ji Y & Wang M, *J Non-Cryst Solids*, 505 (2019) 79.
8 Wang Q, Li X, Fen W, Ji H, Sun X & Xiong R, *J Porous Mater*, 21 (2014) 127.
9 Zu G, Shen J, Zou L, Zou W, Guan D, Wu Y & Zhang Y, *Micro Meso Mater*, 238 (2017) 90.
10 Gao H, Zhang Z, Shi Z, Zhang J, Zhi M & Hong Z, *J Sol-Gel Sci Technol*, 85 (2018) 567.
11 Wang X, Wu Z, Zhi M &Hong Z, *J Sol-Gel Sci Technol*, 87 (2018) 734.
12 Zu G, Shen J, Wang W, Zou L, Lian Y, Zhang Z, Liu B & Zhang F, Robust, *Chem Mater*, 26 (2014) 5761.
13 Xiong R, Li X, Ji H, Sun X & He J, *J Sol-Gel Sci Technol*, 72 (2014) 496.
14 Zhang Z, Gao Q, Liu Y, Zhou C, Zhi M, Hong Z, Zhang F & Liu B, *RSC Adv*, 5 (2015) 84280.
15 Wang X, Li C, Shi Z, Zhi M & Hong Z, *RSC Adv*, 8 (2018) 8011.
16 Zhang Z, Gao Q, Gao H, Shi Z, Wu J, Zhi M & Hong Z, *RSC Adv*, 6 (2016) 112620.
17 Gao Q, Wang X, Shi Z, Ye Z, Wang W, Zhang N, Hong Z & Zhi M, *Chem Eng J*, 331 (2018) 185.
18 Guo X, Song J, Ren J, Yang F, Kanamori K & Nakanishi K, *J Porous Mater*, 23 (2016) 867.
19 Akhtar M N, Chen Y C, AlDamen M A & Tong M L, *Dalton Trans*, 46 (2017) 116.
20 Shi R H, Zhang Z R, Fan H L, Zhen T, Ju S & Mi J, *Appl Surf Sci*, 394 (2017) 394.
21 Sahiner N, Demirci S & Yildiz M, *J Electron Mater*, 46 (2017) 790.
22 Lavoine N, Bras J, Saito T & Isogai A, *J Polym Sci Part A: Polym Chem*, 55 (2017) 1750.
23 Xiong R, Li X, Ji H, Sun X & He J, *J Sol-Gel Sci Technol*, 72 (2014) 496.
24 He J, Li X, Su D, Ji H, Zhang X & Zhang W, *J Mater Chem A*, 4 (2016) 5632.
25 Pyen S, Hong E, Shin M, Suh Y W & Shin C H, *Mol Catal*, 448 (2018) 71.
26 Chao X, Yuan W, Shi Q & Zhu Z, *J Sol-Gel Sci Technol*, 80 (2016) 667.
27 Zhong L, Chen X, Song H, Guo K & Hu Z, *RSC Adv*, 4 (2014) 31666.
28 Mejri I, Younes M K & Ghorbel A, *J Sol-Gel Sci Technol*, 40 (2006) 3.
29 Fenech J, Viazzi C, Bonino J P, Ansart F & Barnabé A, *Ceram Int*, 35 (2009) 3427.